COMPARATIVE POROSITY MEASUREMENTS ON CERAMIC MATERIALS

Robert Sobott[1]*, Klaus Bente[2] and Mario Kittel[1]

[1] GeoZentrum Nordbayern, Friedrich-Alexander-University, Schlossgarten 5, 91054 Erlangen
[2] Institute for Mineralogy, Crystallography and Material Sciences, University Leipzig, 04275 Leipzig
** Corresponding author. Email: ffbd-sobott@t-online.de*

Introduction

Among the various criteria which can be used to classify ceramics are the material and physical properties they inherit from the raw material and the technical processes of forming and firing. The production history is reflected by the chemical and mineralogical phase composition, porosity and pore size distribution. The determination of this data which is usually achieved by classical mineralogical analytical methods can become a challenge if the results have to be obtained from non-destructive methods. X-ray diffractomometry (μ-XRD²), energy dispersive X-ray fluorescence spectroscopy (μ-EDXRF), and X-ray micro computed tomography (X-ray μCT) are three important analytical tools to meet this challenge. This study focuses on porosity, i.e. the different methods of measurement. As porosity is a very important parameter of oil- and gas-bearing sedimentary rocks the determination is extensively practiced in petrophysical laboratories of oil- and gas-producing companies all over the world and an innumerable amount of publications about this subject originates from there. If ceramics are regarded as thermally metamorphosed mudrocks, the application of mineralogical and petrophysical investigation methods for their study becomes obvious.

Three macroscopically different sherds were subjected to a number of analytical methods for the determination of porosity and correlated data such as bulk density, pore size distribution, specific surface, and permeability. The results are compared and discussed with respect to the value of porosity as a parameter for classifying ceramics.

Porosity in ceramics

Porosity in ceramic materials is partly determined by physical and chemical reactions in the course of drying and firing the clay paste. The first important phase of pore space formation sets in with the drying of the wet clay at room temperature when the water of plasticity evaporates. The drying process goes along with a shrinking of the clay paste and a rearrangement of particles. A further increase in porosity is effected by the desorption and evaporation of water on clay and temper particles in the low temperature firing interval between 100 and 200°C, rendering the clay completely dry and creating a mass of particles with interstitial pores. With the removal of all absorbed water, a continued increase in porosity can only be achieved by chemical reactions in which the sum of the volumes of the solid products is smaller than that of the educts. Such reactions are the dehydroxylation of clay minerals, the dissociation of carbonate minerals (calcite, dolomite) and, to a lesser effect, reactions between constituent mineral phases. These reactions take place in the temperature range from 400 to 800°C before the onset of partial melting (Cultrone *et al.* 2001). The absolute changes in porosity at temperatures above 400°C depend on the chemical composition of the clay. Clays with appreciable amounts of carbonate minerals (calcite, dolomite) show a distinct gain in porosity. The dissociation of calcite and the reaction of CaO with SiO_2 to wollastonite is accompanied by an increase in free volume of 33% relating to the sum of the volumes of the educts. In the case of the reaction of dolomite with SiO_2 to diopside and carbon dioxide this gain in free volume amounts even to 40%. The increase in free volume is much smaller or even insignificant, however, if calcite and/or dolomite contents in the clay are low or absent. The dehydroxylation of kaolinite to metakaolinite, SiO_2 and water effects a free volume increase of about 5%, the reaction of muscovite and SiO_2 to sanidine, mullite, and water in the absence of calcite one of 2% (Cultrone *et al.* 2001).

Reactions between anhydrous silicate phases and the formation of melt at temperatures above 800°C lead to a decrease in open porosity. As for example, in the reaction of gehlenite and SiO_2 to wollastonite and anorthite the sum of the volumes of the products is greater by 2.6% than the sum of the volumes of the educts which means that pore space is eliminated. With the firing temperature rising above 800°C the amount of melt increases and the processes taking place in the ceramic can be regarded as liquid phase sintering. Interconnected pores of irregular shape are first surrounded and then filled with melt. While smaller pores are filled completely and vanish larger

pores remain open but take on a globular shape due to interfacial tension effects (Noll 1991). The final state of the ceramic fabric depends on the peak temperature and the course and duration of the firing process and can vary from non-vitrified to completely vitrified. The porosity changes in ceramic materials as a function of the firing temperature are reflected by corresponding density changes. Experimental work by Xu (2013) with carbonate-free clay shows a decrease of the bulk density from 1.83 g/cm³ at 100°C to 1.48 g/cm³ at 800°C and an increase to 1.93 g/cm³ at 1200°C.

Sample material

Two of the three sherds have a known archaeological background and originate from the excavation at Uivar, Romania, and Mfomakap, Cameroon, respectively. The origin of the third sample is unknown. As the work is focused on the comparison of analytical methods and not on the provenance of samples, it was deemed permissible to include it also in this study.

Prior to the measurement of pore-related data the phase composition of each sherd was determined by X-ray diffractometry and optical microscopy. The optical microscopy study was made with thin sections of 20 μm thickness. The samples were prepared from slices of about 1 mm thickness cut off from the sherds. The rapid recognition of pores was supported by filling them with a blue-dyed epoxy resin by vacuum-impregnation at the beginning of the preparation process.

Sample No. 1 from Uivar, Romania

The sample from Uivar is a body sherd attributed to the Szakálhát group of the eastern Neolithic linear pottery culture (Dammers 2012; Figure 1). The crystalline phase composition includes an assemblage of quartz + plagioclase which can be typical for a carbonate-free raw material.

The crystalline phase composition of the sherd is made up of quartz + plagioclase (+ orthoclase?) + biotite + muscovite. The firing temperature of the ceramic made from a carbonate-free raw material is estimated to have lain in the interval 850-900°C according to SEM photographs showing traces of vitrification (Maniatis and Tite 1981).

Figure 1 shows the typical orange-red colour of the sherd as the result of firing under oxidising conditions and a decoration by deep grooves on the exterior side. The optical microscopy of a thin section reveals that besides inorganic material organic matter was used as temper.

Sample No. 2 from Mfomakap, Cameroon

The sample from Mfomakap is a rim sherd and also of (African) Neolithic age (Epossi 2012). It is characterised microscopically by a coarse-grained temper which includes a diagnostic heavy mineral fraction consisting of cyanite, garnet, and rutile (Figure 2).

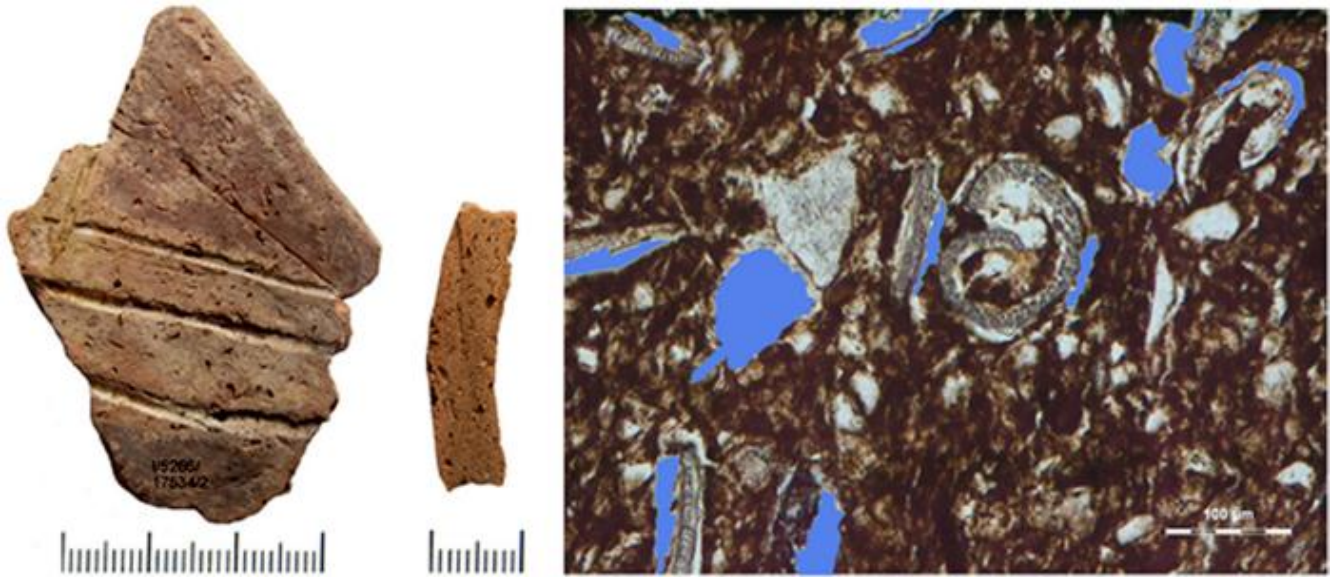

Figure 1. Left: exterior side and cross section of sample 1 with clearly visible macroscopic pores (blue coloured areas on the right). Right: thin section perpendicular to the surface of the sherd with organic temper almost in the centre.

Figure 2. Left: exterior side and cross section of sample 2 with macroscopically visible temper grains and pores. Right: thin section perpendicular to the surface of the sherd with quartz (white irregular grains), biotite (brown), muscovite (lath-shaped, white crystals) and cyanite (with traces of cleavage planes) in the centre. The pore space is coloured in blue.

Sample No. 3 of unknown origin

The third sample is a bottom sherd. The crystalline phase assemblage comprises quartz, plagioclase, and diopside. Unlike the other two samples this sherd originates from a vessel which was made from a carbonate-rich clay. The presence of diopside and absence of gehlenite and the orange-red colour point out to a firing temperature interval of 900-1000°C under oxidising conditions (Noll 1991). The thin section (Figure 3) reveals a fairly uniform grain and pore size distribution.

Measurement of porosity and related petrophysical data

Porosity is defined as the quotient of the pore volume and total volume (= matrix volume + pore volume) of a porous material. The pore volume is made up of pores of different size and geometry which may be either interconnected and accessible from the exterior (predominantly interparticle pores) or isolated (intraparticle pores). The distribution of pores may be isotropic or anisotropic, for instance as elongated pores aligned in a parallel direction. Pore sizes usually encountered in ceramic materials range from 1 nm to 1 mm and encompass micropores (< 2 nm) to macropores (> 50 nm). This range of pore sizes spanning 10^6 cannot be covered by a single method for porosity measurement and depending on the range of interest various methods are applied (Figure 4).

The so-called direct methods measure the volume of a liquid or a gas filling the pore volume under fixed pT (pressure, Temperature) conditions and the result is presented as a numerical value (Archimedes' Principle, mercury porosimetry, capillary condensation). Penetrating fluids may be alcohol (isopropanol), mercury or nitrogen. The data evaluation is straightforward in the case of the Archimedes' Principle where the porosity is equal to the quotient of m_1 and $m_1 + m_2$, m_1 being the mass of the fluid filling the pore space completely and m_2 the mass of the fluid displaced by the matrix. Additional information furnished by this method are the matrix and bulk density which can be used to check the plausibility of the measurement.

Mercury porosimetry takes advantage of the capillary pressure equation which states that the pressure needed to fill a pore with mercury is inversely proportional to the pore size (León y León 1998; Giesche 2006). This method yields not only the absolute pore volume (porosity) of a sample but also the pore size distribution because the pressure is increased in incremental steps to its final value, and the corresponding incremental mercury volumes are recorded in the measurement. Capillary condensation follows a similar principle where the condensation of a gas (nitrogen) in a capillary depends on the vapour pressure and is described by the Kelvin equation (Harry and Johnson 2004). It is obvious that the direct methods capture only the interconnected pores which are accessible from the exterior.

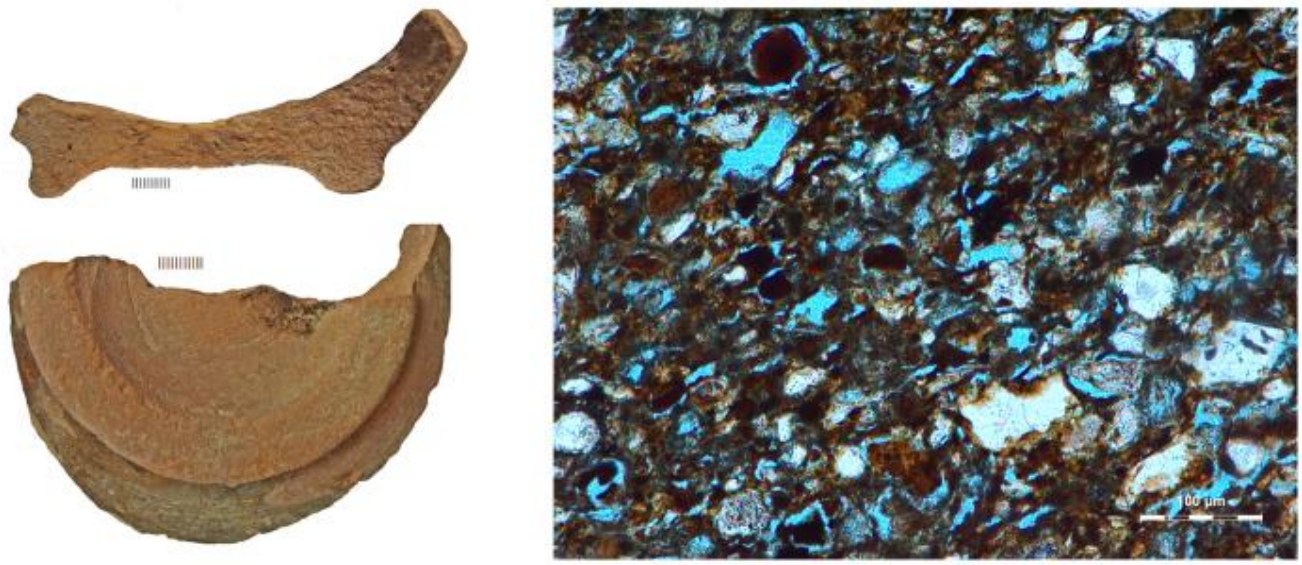

Figure 3. Left: exterior side and cross section of sample 3. Right: thin section parallel to the cross section of the sherd displaying uniform grain and pore size distribution.

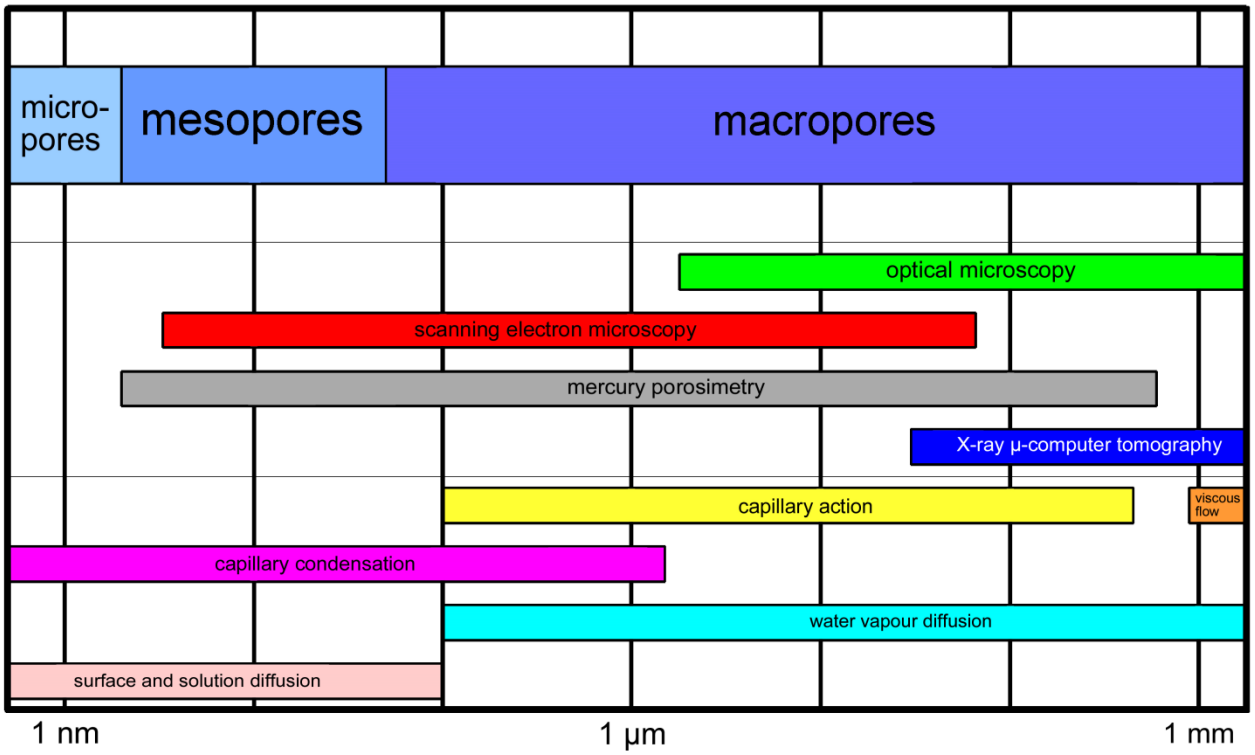

Figure 4. Pore size range in ceramics and relevant methods of measurement and corresponding physical processes.

Indirect methods of porosity measurement produce a 2D or a 3D image of the porous structure (optical microscopy [Riederer 2004] and scanning electron microscopy [Freestone and Middleton 1987], X-ray µ-computed tomography [Kahl and Ramminger 2012]), which is subsequently evaluated by image analysis software with respect to porosity.

It is obvious that porosity values obtained from direct and indirect methods for a sample are different and depend on the physics of the underlying principle of measurement. Non-destructive methods

such as the Archimedes' Principle, capillary condensation and X-ray μ-computed tomography are specially suited for the investigation of archaeological samples.

The range of pore sizes encountered in ceramics is shown in Figure 4 together with relevant methods of investigation and measurement and corresponding physical processes. Mercury porosimetry covers almost the complete range of mesopores and macropores and is well suited for the measurement of porosity and pore size distribution. From the plot of mercury saturation S_{Hg} in the sample versus capillary pressure P_c (capillary pressure curve) the permeability of the porous material can be calculated according to the procedure given by Marshall (1958). Based on various pore shape models (cylindrical, parallel plate) the mercury porosity data allows also the calculation of the specific surface area of the porous material which may be checked by the result obtained from the nitrogen adsorption isotherm measurement (Brunauer-Emmett-Teller, BET specific surface area). The four most important parameters for the characterisation of the pore space of a ceramic, absolute porosity, pore size distribution, specific surface area, and permeability, can thus be obtained from the evaluation of one measurement. Unfortunately this method converts the sample after the completion of the measurement into toxic waste.

This explains why mercury porosity is not so extensively applied as the results would recommend. Especially with a view to the integrity of the sample alternative methods are considered. However, these are heavily restricted as far as the resolution and information values are concerned.

The Archimedes' Principle yields only the absolute porosity, by the capillary condensation method the larger part of the macropores is not covered and X-ray μ-computer tomography applied to representative sample sizes with several cubic centimetres volume does not resolve the range from the medium part of the macropores to the micropores. The resolution, defined by the cell edge length of a voxel, for samples of cm-size is about 30 μm which means that pores with smaller cross sections are not recognized. On the other hand, for a resolution of 0.06 μm the sample size should not be greater than 5 mm which will be much too small for a representative sample in most cases.

Comparative measurements on samples 1, 2 & 3

Bulk and matrix density, porosity, specific surface area, and pore size distribution of all three samples were determined by the Archimedes' Principle, mercury porosimetry, and the BET method, respectively. The measurements were carried out with a Sartorius LA310S balance with the YDK01 density kit (Archimedes' Principle), the Quantachrome PoreMaster 60 (mercury porosimetry), and the Quantachrome Autosorb iQ (BET surface area). The permeability was calculated from the plot of mercury saturation in the sample versus capillary pressure. All measured data is summarized in Table 1.

To facilitate the comparison of pore size distributions the histogram presentation of the pore size distribution (PSD) was replaced by the continuous function:

$$y = \sum_{n=1}^{21} a_n e^{-b_n (x-c_n)^2} \quad 0 \le x \le 6)$$

which was adjusted by matching the area under the curve with the summed up area of the histogram bars. The curve fit was accepted when the difference between the area values was less than 5%. A further check was made by calculating the capillary pressure curve from the PSD function and evaluating it with respect to permeability and compare that value with the one obtained from the measured capillary pressure curve. The graphs of the PSD functions for the three samples are shown in Figure 5. The inset top left shows the match of the PSD function to the histogram bars for sample 3. The continuous function has the further advantage over the histogram presentation that maximum and HWHM values can be easily evaluated and used for the statistical analysis of the PSD of ceramics.

In the case of sample 3 the standard measurements were supplemented by an X-ray μCT study. The investigation was made with an installation of the Institute of Non-Destructive Testing (IKTS-MD) of the Fraunhofer Society in Dresden/Saxonia at the Institute of Mineralogy, Crystallography, and Material Science of the University Leipzig with a direct beam tungsten target X-ray tube which was operated at 170 kV and 120μA in the high power mode with a 0.5 mm Cu filter. The images were recorded with a Perkin Elmer flat panel detector XRD 1621 CN. The programme module "defect analysis" of the Volume Graphics Studio Max 2.0 software was used for the data evaluation with regard to porosity.

	Bulk Density [g/cm³]			Matrix Density [g/cm³]			Porosity [Vol. %]			Specific Surface [m²/g]		Permeability [mD]
	AP	Hg	CT	AP	Hg	CT	AP	Hg	CT	BET	Hg	
Sample 1	1,42	1,42	—	2,53	2,62	—	44,1	45,8	—	1,88	5,88	67,6
Sample 2	1,82	1,80	—	2,55	2,42	—	28,7	25,6	—	64,2	14,4	20,9
Sample 3	1,67	1,64	2,05	2,72	2,62	2,27	38,7	37,5	7,4	11,8	7,4	9,3

Table 1. Petrophysical data for samples 1, 2 and 3. AP: Archimedes' Principle, Hg: Mercury porosimetry, CT: X-ray μ-computer tomography, BET: BET specific surface area.

The arbitrary parameters grey level, defect size, and defect probability were adjusted in such a way that a maximum of pores were identified by the software. If the defect size is chosen too small, large pores will not be identified (Figure 6) and the defect size has to be enlarged accordingly. The voxel's edge length was calculated from the quotient of total pore volume and corresponding total voxel number and amounts to 30 μm. It is obvious that with this voxel size the predominant pore sizes <10 μm cannot be detected and the calculated porosity which takes only pore sizes >30 μm into account must be too small.

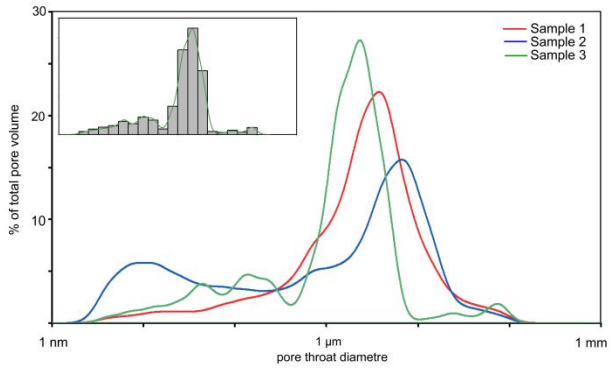

Figure 5. Pore size distributions of the samples 1, 2 and 3 from mercury porosimetry (inset diagram shows the transformation of the bar diagram for sample 3 into the graph of a continuous function).

Consequently the calculated values for the bulk and matrix densities are too high and low, respectively (see Table 1). On the other hand, the strong points of the CT are the presentation of pictures indicating the 3D orientation of pores and quick information about the pore size distribution of pores larger than the voxel size. The 3D imaging of pores also reveals how much or how little the actual pore geometry has in common with the idealised models of cylindrical and parallel plate pores. An example for the preferred orientation of pores is shown in the he upper left photograph in Figure 6. The stretched pores are aligned in a 160° direction. The blue and green colours indicating the pore volume size corroborate the uniform pore size distribution already noticed in the thin section (Figure 3).

Meanwhile μCT has been overtaken by n(ano)CT but the principle problem remains: higher resolution must be paid for with lower representativeness of the sample. If a resolution of 60 nm can only be obtained for a sample not bigger than 5 mm then nCT makes sense only for very fine-grained ceramics as for example *terra sigillata*.

Discussion

Like chemical and mineralogical phase data, information about the pore system is so characteristic that it can be used for the classification of ceramics. However, it is not the single value of porosity that classifies a sample but the PSD in combination with other data relevant for the description of pore space such as the specific surface area and permeability. Moraru and Florica (2011) used PSD for the discrimination of archaeological and faked pottery artefacts. They also employed ultrasonic measurements to investigate the porous structure and mechanical properties (Young's modulus) of ceramic materials (Moraru and Szendrei 2010). The approach to measure several petrophysical parameters of samples makes sense as they are linked together and it allows a check of the data for consistency. For instance, the bulk density is inversely proportional to the porosity, the specific surface is inversely proportional to medium pore radius defined as the quotient of total pore volume and specific surface area, the Kozeny-Carman equation (Engelhardt 1960) links permeability to porosity and specific surface, the Wyllie time-average-equation relates the ultrasonic velocity to the porosity of a porous material (Wyllie *et al.* 1956), etc. As the information pertaining to the PSD is contained in the capillary pressure curve, which is the basis for the calculation of permeability, a triple of the petrophysical parameters permeability, specific surface area, and porosity is well suited to characterise a ceramic sample unambiguously. As porosity is also directly

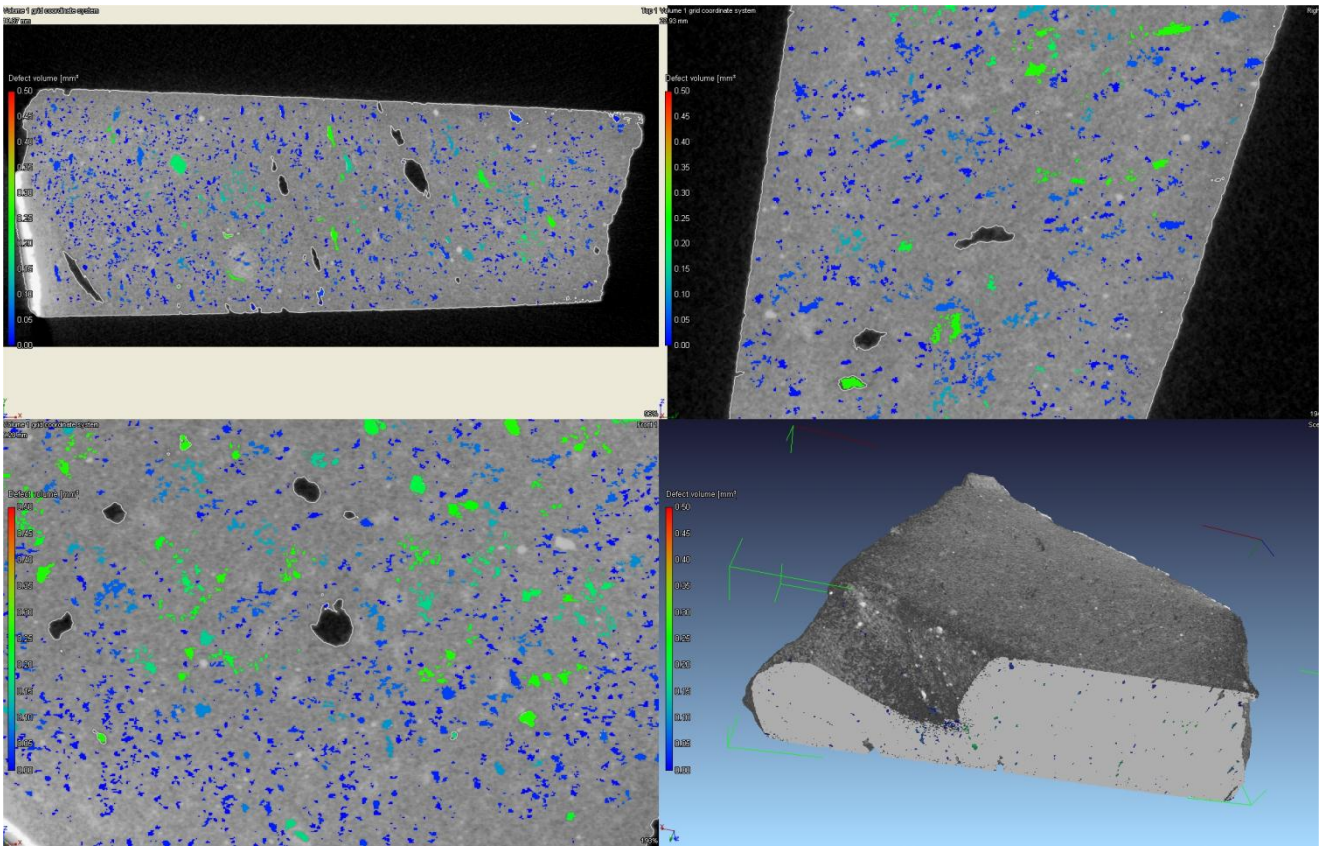

Figure 6. Computed tomographic slices of sample 3 (bottom right). Pores are coloured according to the pore volume size (see explanation for the black areas in the text).

and/or indirectly linked to the mechanical properties, the raw material composition and firing parameters, the data can be used to suggest the functionality of the ceramics and choice of raw materials and manufacturing processes by the potter. In connection with X-ray diffraction phase analysis porosity data can assist to differentiate between ceramics fired at high temperature, stoneware (proto-porcelain) and porcelain proper.

A check of the data in Table 1 yields a satisfactory agreement for the bulk density and porosity determined by Archimedes' Principle and mercury porosimetry for all samples. The agreement is less satisfactory for the matrix density. The distinct differences in the BET and modelled specific surface areas are due to discrepancies between the pore models and the real pore structure and geometry. The BET value for sample 2 is inexplicably high and does not fulfill the data consistency check. As mentioned earlier the quality of petrophysical parameters derived from μCT data needs to be complemented as the strong point of μCT is the imaging and not the quantification of the pore space.

Conclusion

The next step should be the test to link petrophysical data to certain types of ceramics with respect to grain size and temper, carbonate content of the raw material, and the firing conditions (low, medium, high temperature; oxidising, reducing conditions). Sample 2 represents a ceramic which is coarse-grained/tempered and was produced from a carbonate-free clay and fired at medium to high temperatures under oxidising conditions while sample 3 stands for a fine-grained/non-tempered ceramic, which was produced from a carbonate-rich clay, and fired at high temperature under oxidising conditions. The high porosity of sample 3 could be partly due to the dissociation of carbonate minerals. Fine-grained and evenly distributed carbonate minerals in the clay matrix would also explain the fairly uniform PSD which is reflected by a pronounced maximum and narrow HWHM. On the other hand, the coarse-grained temper in sample 2 is probably the cause for larger intraparticle pores which shifted the PSD to larger pore throat diameters with the consequence of a higher permeability. The results from these two examples

show that although this type of study is in its initial phase, it addresses a new direction into which further studies should go to help characterise ceramic technology, function and different workshop manufacturing processes.

References

Cultrone, G., Rodriguez-Navarro, C., Sebastian, E., Cazalla, O. and De La Torre, M. J. 2001. Carbonate and silicate phase reactions during ceramic firing. *European Journal of Mineralogy* 13, 621-634.

Dammers, B., Franz, A., Sobott, R. and Bente, K. 2012. Erste Ergebnisse archäometrischer Untersuchungen zur mittel- und spätneolithischen Keramik von Uivar (Rumänien) unter besonderer Berücksichtigung der 3D-µ-Röntgen-Computertomographie. In Ramminger, B. and Stilborg, O. (eds.) *Naturwissenschaftliche Analysen vor- und frühgeschichtlicher Keramik II. Universitätsforschungen zur prähistorischen Archäologie (Bonn 2012)* 216, 33-57.

Engelhardt von, W. 1960. Der Porenraum der Sedimente. Springer-Verlag, Berlin.

Epossi Ntah, E. L. 2012. *Archaeometrical studies: petrography, mineralogy and chemistry of selected ceramic sherds and clay samples from Cameroon in the Regions of Mombal, Mfomakap and Zamala.* Ph. D. Thesis, University of Leipzig.

Freestone, I. C. and Middleton, A. P. 1987. Mineralogical applications of the analytical SEM in archaeology. *Mineralogical Magazine* 51, 21-31.

Giesche, H. 2006. Mercury porosimetry: a General (Practical) Overview. *Particle and Particle Systems Characterization* 23, 1-11.

Harry, K. G. and Johnson, A. 2004. A non-destructive technique for measuring ceramic porosity using liquid nitrogen. *Journal of Archaeological Science* 31(11), 1567-1575.

Kahl, W. A. and Ramminger, B. 2012. Zerstörungsfreie Analysen prähistorischer Keramik mittels hoch auflösender Mikro-Computertomographie am Beispiel spämesolithischer und neolithischer Funde aus Hamburg-Boberg. In Ramminger B. and Stilborg, O. (eds.) *Naturwissenschaftliche Analysen vor- und frühgeschichtlicher Keramik II.* niversitätsforschungen zur prähistorischen Archäologie 216, 59-95. Bonn.

León y León, C. A. 1998. New perspectives in mercury porosimetry. *Advances in Colloid and Interface Sciences* 76/77, 341-372.

Maniatis, Y. and Tite, M. S. 1981. Technological Examination of Neolithic-Bronze Age Pottery from Central and Southeast Europe and from the Near East. *Journal of Archaeological Science* 8, 59-76.

Marshall, T. J. 1958. A relation between permeability and size distribution of pores. *Journal of Soil Science* 9 (1), 1-8.

Moraru, L. and Szendrei, F. 2010. Ultrasonic properties of ancient ceramic materials with porous structure. *Journal of Science and Arts* 2 (13), 345 -348.

Moraru, L. and Szendrei, F. 2011. Structural features of archaeological pottery. *Journal of Engineering Studies and Research* 4 (17), 73-78.

Noll, W. 1991. *Alte Keramiken und ihre Pigmente. Studien zu Material und Technologie*. E. Schweitzerbart'sche Verlagsbuchhandlung, Stuttgart.

Riederer, J. 2004. Thin section microscopy applied to the study of archaeological ceramics. *Hyperfine Interactions* 154, 143-158.

Wyllie, M. R. J., Gregory, A. R., and Gardner, L. W 1956. Elastic wave velocities in Heterogeneous and porous media. *Geophysics* 21(1), 41-70.

Xu, W. 2013. Vergleich mineralogischer Methoden zur Bestimmung der Brenntemperaturen von Keramik anhand von Brennexperimenten mittelalterlicher Keramik aus den Mayener „Burggärten" (Comparison of mineralogical methods for the determination of firing temperatures of ceramics by firing experiments with medieval ceramics from the Mayener "Burggärten"). In B. Ramminger, B. and Stilborg O. (eds.) *Naturwissenschaftliche Analysen vor- und frühgeschichtlicher Keramik III,* 238, 173-188. Universitätsforschungen zur prähistorischen Archäologie (Bonn 2013).